Control of Nanoparticles with Arbitrary Two-Dimensional Force Fields

Adam E. Cohen*

Department of Physics, Stanford University, 382 Via Pueblo Mall, Stanford, California 94305, USA

An anti-Brownian electrophoretic trap is used to create arbitrary two-dimensional force fields for individual nanoscale objects in solution. The trap couples fluorescence microscopy with digital particle tracking and real-time feedback to generate a position-dependent electrophoretic force on a single nanoparticle. The force may vary over nanometer distances and millisecond times and need not be the gradient of a potential. As illustrations of this technique, I study Brownian motion in harmonic, power-law, and double-well potentials.

Feedback control is widely used to stabilize the motion of stochastic systems, where the stochasticity may arise from quantum, thermal, or manufacturing fluctuations. In particular, feedback may be used to cancel the Brownian motion of a single nanoscale object in solution, over some finite bandwidth. This principle has been applied to trapping of micron-sized objects where the feedback force is magnetic [1] or optical [2]. Enderlein [3] and Berglund and Mabuchi [4] recently proposed using feedback to track the Brownian motion of individual fluorescent molecules in solution. For nanoscale objects, electrophoretic forces are far stronger than either magnetic or optical forces and are thus more amenable to inclusion in a feedback system. Here I experimentally demonstrate real-time feedback electrophoresis as a means to control the motion of individual nanoscale objects in solution.

The first part of this Letter describes the experimental apparatus. Parts two through four describe experiments on nanoparticles of various sizes in potentials of various shapes: a 50 nm nanoparticle in a harmonic potential, a 200 nm nanoparticle in a power-law potential, and a 200 nm nanoparticle in a double-well potential. The nanoparticles used in this study are fluorescent polystyrene (Molecular Probes, Eugene, OR, USA), diluted in distilled water, and used under ambient conditions.

A microfluidic cell forms the heart of the anti-Brownian electrophoretic (ABEL) trap (Fig. 1). Particles in the trapping region diffuse freely in the x-y plane but are confined to <1 μm in the z direction. A voltage, $\mathbf{V} = (V_x, V_y)$, applied to the control electrodes leads to an electro-osmotic flow in the trapping region with velocity $\mathbf{u} \propto \mathbf{V}$. The flow imparts a force, $\mathbf{F} \propto \mathbf{u}$, to all particles in the trapping region. The maximum flow speed is $u \sim 3$ mm/s.

The sample cell is mounted in an optical microscope and fluorescence images are captured on a high-sensitivity charge-coupled device (CCD) camera (Cascade 512B, Roper Scientific) at frame rates of up to 300 Hz. A personal computer processes the images in real time to extract the in-plane coordinates, $\mathbf{r}(t)$, of a single nanoparticle. The computer then applies a feedback voltage to the electrodes,

calculated from a user-specified function, $\mathbf{V}(\mathbf{r})$. This voltage translates directly into an arbitrary two-dimensional force field for the particle of interest. At the end of a run, the computer provides a record of the trajectory of the particle, $\mathbf{r}(t_n)$, and the feedback voltage, $\mathbf{V}(t_n)$, acquired at times $t_n = t_0 + n\delta t$, where δt is the interval between video frames. A similar apparatus with lower spatial and temporal resolution is described in [5].

In the simplest incarnation of the ABEL trap, the feedback voltage provides a linear restoring force: $\mathbf{V} = -A(\mathbf{r} - \mathbf{r}_0)$, where $\mathbf{r}_0$ is a target position. When the gain A is properly adjusted, the electrophoretic drift between
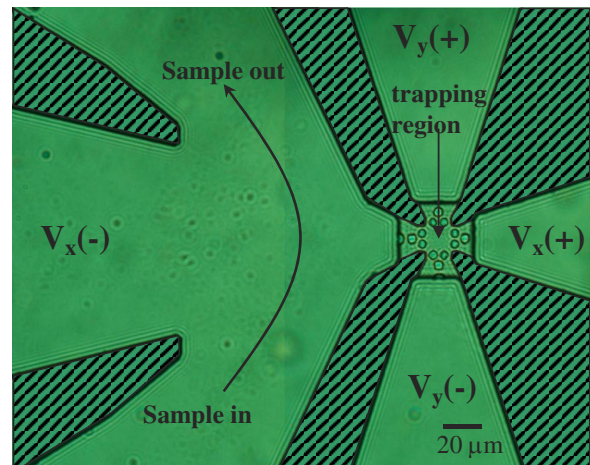
FIG. 1 (color online). Microfluidic cell, formed from an oxidized polydimethylsiloxane (PDMS) stamp and a glass cover slip. The trapping region (~ 20 μm across and 880 nm deep) allows free in-plane diffusion of submicron particles, while confining the particles to the focal plane of the microscope. Small circles surrounding the trapping region are support posts to keep the PDMS from collapsing onto the glass. Microfluidic channels (~ 20 μm deep, ~ 700 μm wide, and ~ 7 mm long) radiate outward from the trapping region and terminate in macroscopic copper electrodes. The channel on the left splits into three to allow for rapid sample delivery. Regions of PDMS in contact with the glass have been crosshatched for clarity.

frames n and $n + 1$ exactly cancels the Brownian displacement between frames $n - 1$ and n, so the particle is trapped at position $\mathbf{r}_0$. Changing $\mathbf{r}_0$ in the software causes the particle to move in two-dimensional space. We have used the ABEL trap in this mode to trap and manipulate individual CdSe nanocrystals, lipid vesicles, molecules of λ-DNA, and particles of tobacco mosaic virus [6].

Figure 2 shows the trajectory of a trapped nanosphere subject to linear feedback. The position fluctuations are Gaussian with rms amplitudes of $\sigma_x = 550$ nm and $\sigma_y = 520$ nm. The effective spring constants are related to the amplitude of the thermal fluctuations via $k = k_B T/\sigma^2$, so $k_x = 1.3 \times 10^{-8}$ N/m, and $k_y = 1.5 \times 10^{-8}$ N/m. Individual nanospheres were held in the trap for periods of up to several minutes.

From the measured trajectory one may reconstruct a pseudo-free trajectory, i.e., a trajectory similar to the one the particle would have followed had it not been trapped. Let the displacement of the particle between adjacent pairs of frames be $\delta\mathbf{r}(n) \equiv \mathbf{r}(n + 1) - \mathbf{r}(n)$. This displacement is related to the applied voltage via

$$\delta r_i(n) = \mu_{ij}^{(0)} V_j(n)\delta t + \mu_{ij}^{(1)} V_j(n + 1)\delta t + \xi_i(n), \quad (1)$$

where the μ_{ij} are 2×2 mobility matrices and $i, j = x, y$. The Langevin term, $\xi_i(n)$, obeys the fluctuation-dissipation relation $\langle \xi_i(n)\xi_j(m) \rangle = 2D\delta t\delta_{ij}\delta_{nm}$, where D is the diffusion coefficient of the particle. The displacement depends on both $\mathbf{V}(n)$ and $\mathbf{V}(n + 1)$ because the voltage switches at a time in between t_n and t_{n+1}. Off-diagonal mobilities arise through nonideal behavior of the trap (e.g., fringing fields or rotation of the trap axes relative to the CCD axes) and are typically small.

The eight coefficients of the mobility matrices are obtained through a multidimensional linear regression of the measured displacements against the applied voltages. The residuals from this fit are the displacements due purely to thermal fluctuations. Summing these residual displacements leads to a pseudo-free trajectory, as illustrated in
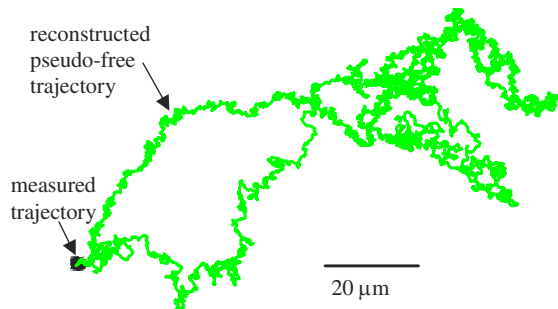
FIG. 2 (color online).   Trajectory of a trapped 50 nm particle, measured over 10 000 time steps (45 s). A "pseudo-free" trajectory is obtained by subtracting from the measured trajectory the motion due to the applied electric field. The pseudo-free trajectory is constrained to start and end at the origin.

Fig. 2. This kind of reconstruction can be performed only with an active trap because it requires a knowledge of the force applied by the trap at all times.

Gosse and Croquette modeled a Brownian particle subject to linear, discrete-time feedback using the Langevin equation [1]:

$$r_i(n + 1) = r_i(n) - \alpha r_i(n - \Delta) + \xi_i(n), \quad (2)$$

where α is a dimensionless measure of the feedback gain and Δ is the feedback delay, measured in video frames. For the present apparatus Δ is between 1 and 2. They showed that a particle subject to Eq. (2) undergoes thermal fluctuations with a power spectrum,

$$|r_i(f)|^2 = \frac{4D\delta t^2}{|e^{2\pi if} - 1 + \alpha e^{-2\pi if\Delta}|^2}. \quad (3)$$

Equation (3) predicts that when α surpasses a threshold (determined by Δ) the power spectrum develops a peak and the particle starts to oscillate. The spectra of Eq. (3) are in quantitative agreement with experiment, both for values of α above and below the oscillation threshold. Figure 3 shows the power spectra of the trapped and pseudo-free trajectories of Fig. 2. The trapped spectrum is well described by Eq. (3), with α just at the oscillation threshold, while the pseudo-free spectrum is fit by $1/f^2$ noise, as expected for a free random walk.
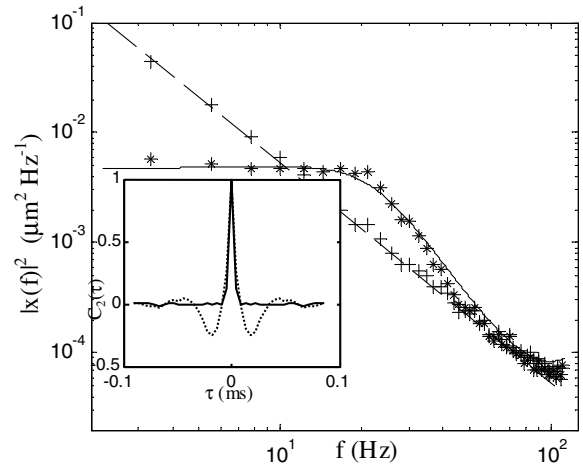
FIG. 3.   Power spectra of the x fluctuations of a trapped 50 nm particle (*) and of the corresponding pseudo-free trajectory (+). The trapped spectrum is fit by Eq. (3), with $\delta t = 4.5$ ms, $\alpha = 0.3$, and $\Delta = 1.3$. The value of D is fixed at the value extracted from the pseudo-free power spectrum (8.7 μm^2 s^{-1}). The pseudo-free spectrum is fit by $|x(f)|^2 = D/(\pi f)^2$. Inset: normalized two-point correlation functions of the displacements between successive frames along the x axis, $C_2(\tau) \propto \langle \delta x(t)\delta x(t + \tau) \rangle$. The correlation function of the measured trajectory (dashed line) shows ringing due to the feedback delay, while that of the pseudo-free trajectory (solid line) shows δ-correlated steps.

Using the diffusion coefficient extracted from the pseudo-free trajectory ($D = 8.7$ $\mu m^2\,s^{-1}$), the Stokes-Einstein relation implies a particle diameter of 50 nm. Nanoparticles in the stock solution had a nominal diameter of 24 ± 4 nm, corresponding to an expected $D = 18 \pm 3$ $\mu m^2\,s^{-1}$. To resolve this discrepancy between the measured and expected values of D, the measurement of Fig. 2 was repeated for $n = 19$ more nanoparticles from the same solution (trapped for 1000 video frames each). The average measured diffusion coefficient was $D = 16 \pm 6$ $\mu m^2\,s^{-1}$ (min 5.7 $\mu m^2\,s^{-1}$ and max 31 $\mu m^2\,s^{-1}$), in reasonable agreement with the expected value. For the nanoparticle with $D = 31$ $\mu m^2\,s^{-1}$ the Stokes-Einstein relation yields a diameter of 14 nm.

Now let us turn to motion in nonlinear force fields. With a trivial modification of the software, it is possible to apply an arbitrary $\mathbf{V}(\mathbf{r})$ to a single particle. Consider a feedback voltage of the form

$$\mathbf{V} = -A\left(\frac{r}{r_0}\right)^\beta \hat{r}. \tag{4}$$

The particle experiences an effective potential proportional to $r^{\beta+1}$, or to $\ln r$ for $\beta = -1$. Thus the potential is harmonic for $\beta = 1$, conical for $\beta = 0$, logarithmic for $\beta = -1$, and Coulombic for $\beta = -2$. When $-1 < \beta \leq 0$, the potential has a cusp at $r = 0$. When $\beta \leq -1$, the potential diverges at $r = 0$, and when $\beta < -1$, the potential is bounded as $r \to \infty$. At any finite temperature, a particle will be stably trapped only for $\beta > -1$.

A single 200 nm particle was subjected to 15 different values of β between -0.8 and 4. For each value of β, 10 000 frames of data (roughly 45 s) were acquired. For $-1 < \beta < -0.8$ the fluctuations in position were large enough to take the particle out of the field of view, preventing extended observations.
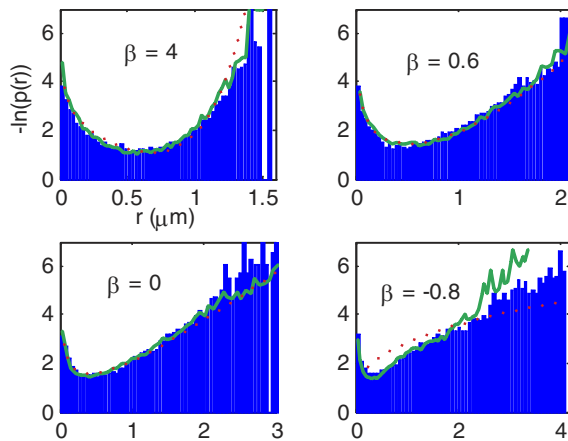
FIG. 4 (color online).   Radial probability distributions [plotted as $-\ln p(r)$] for a 200 nm particle in a power-law potential. Blue bars: measured distribution; red dots: Eq. (5); green line: numerical simulation.

The radial distribution function of a particle subject to restoring the force of Eq. (4) is

$$p(r) \propto r \exp\left(\frac{-Ar(\frac{r}{r_0})^\beta}{(\beta+1)k_BT}\right), \tag{5}$$

where the normalization is given by the constraint $\int_0^\infty p(r)dr = 1$. Figure 4 compares the predictions of Eq. (5), plotted as $-\ln p(r)$, with the measured radial probability distribution for several values of β. The agreement is good for $\beta > -0.4$. To account for the disagreement when $\beta < -0.4$, Brownian dynamics simulations were performed for a particle subject to the restoring force of Eq. (4), taking into account the feedback latency of 1.6 video frames. Including the effect of delay led to excellent agreement between theory and experiment. The feedback delay becomes most significant as $\beta \to -1$ and $r \to 0$ because the restoring force becomes increasingly kinked near the origin.

As a final illustration of the ABEL trap, a 200 nm particle was subjected to a force field corresponding to a double-well potential. The feedback voltage is

$$\mathbf{V}(\mathbf{r}) = (k_x x - \gamma x^3)\hat{x} - k_y y\hat{y}. \tag{6}$$

Hopping rates are obtained by fitting the data with a hidden Markov model, in which the two "hidden" states correspond to the particle residing in one or the other minima of the potential. Each hidden state is assumed to generate Gaussian-distributed observations of the position of the particle.
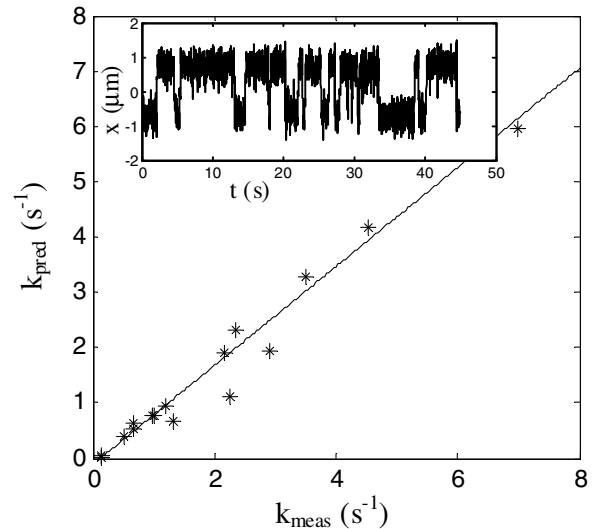
FIG. 5.   Comparison of experimental and theoretical hopping rates for a 200 nm particle in a double potential well. Eight trajectories were acquired (10 000 data points each), leading to 16 experimental rates (left $\rightarrow$ right and right $\rightarrow$ left for each trajectory). The trend line has a slope of 0.89 (ideal $= 1$), which is reasonable given the uncertainties in the size of the particle. Inset: the representative trajectory of a single particle.

The Kramers theory predicts that the hopping rate, W, in a potential double well is given by [7]

$$W = \frac{\sqrt{|k_s||k_1|}}{2\pi\Gamma} e^{-\Delta U/k_B T}, \qquad (7)$$

where k_s and k_1 are the curvatures of the potential along the reaction coordinate at the saddle point and the starting minimum, respectively. $\Gamma = 6\pi\eta a$ is the drag coefficient of the particle, where η is the viscosity and a is the radius, and ΔU is the potential of the saddle point relative to the starting minimum. The parameters k_s, k_1, and ΔU are, in principle, determined by the feedback parameters k_x and γ. However, a slight fluid drift during the experiments tended to bias the particle towards one potential well over the other. Better agreement between the measured hopping rates and Eq. (7) was obtained when k_s, k_1, and ΔU were extracted from the measured distribution of particle positions, assuming that the distribution was related to the potential via a Boltzmann distribution. Figure 5 compares the measured hopping rates with the predictions of Eq. (7). McCann *et al.* have performed much more accurate tests of the Kramers theory using silica particles in a double optical trap [8].

It is interesting to compare the scaling of the performance of the ABEL trap with particle size to that of optical tweezers. A particle held in the ABEL trap undergoes fluctuations with mean-square amplitude $\sigma^2 \sim 2Dt_r$ along each axis, where t_r is the response time of the feedback loop. These fluctuations correspond to an effective spring constant $k_{\text{eff}} = k_B T/\sigma^2$. Since $D \propto a^{-1}$, where a is the radius of the particle, we have $k_{\text{eff}} \propto a$. In contrast, the interaction in optical tweezers scales with the *volume* of the particle, so the spring constant is $k_{\text{opt}} \propto a^3$. Optical tweezers require ever stronger fields to trap smaller objects; the ABEL trap requires faster feedback. While intense lasers run into problems with heating and photodamage, we note that the bandwidth achieved in the present study is fairly modest. More sophisticated tracking schemes [3,4] may push the bandwidth up to several kHz, in which case it should be feasible to trap objects of order 1 nm in diameter. Ultimately photon statistics will limit the ABEL trap: it is impossible to know the location of an object in between detecting photons from it. Photons from single molecules are routinely detected with count rates $>5000 \text{ s}^{-1}$.

Curtis *et al.* have demonstrated complex static and time-dependent configurations of optical traps, which can be used to investigate effects similar to the ones discussed in this Letter [9]. There are several differences between the ABEL trap and a multibeam optical trap: (i) The ABEL trap always traps exactly one particle: the Brownian motion of distinct particles is uncorrelated, so the force used to cancel the Brownian motion of one particle augments the Brownian motion of all others. An optical trap creates a genuine spatially varying potential which exerts different forces on distinct particles and may trap more than one particle. (ii) The ABEL trap requires an electrically homogeneous medium, while an optical trap requires an optically homogeneous medium (although both can tolerate some level of disorder). (iii) The ABEL trap provides a record of the forces exerted on a particle, while an optical trap does not. (iv) The ABEL trap exerts uniform forces, while an optical trap may exert force gradients. Thus a polymer trapped in the ABEL trap maintains its free solution conformation, while a polymer trapped in an optical trap is compacted. (v) The ABEL trap can manipulate objects far smaller than can be manipulated with optical tweezers. The ABEL trap promises to be most useful for manipulating small (<100 nm) or delicate objects in solution which cannot currently be manipulated in any other way.

In this Letter I have presented a few simple force fields to illustrate the ABEL trap. However, it should be noted that force fields of practically arbitrary complexity can be constructed. Such force fields may be useful for studying diffusion in lattices, in the presence of static or dynamic disorder, or in time-varying fields. Furthermore, such force fields may be useful in sorting or assembling nanoscale components.

*Electronic address: acohen@post.harvard.edu
[1] C. Gosse and V. Croquette, Biophys. J. **82**, 3314 (2002).
[2] K. C. Neuman and S. M. Block, Rev. Sci. Instrum. **75**, 2787 (2004).
[3] J. Enderlein, Appl. Phys. B **71**, 773 (2000).
[4] A. J. Berglund and H. Mabuchi, Appl. Phys. B **78**, 653 (2004).
[5] A. E. Cohen and W. E. Moerner, Appl. Phys. Lett. **86**, 093109 (2005).
[6] A. E. Cohen and W. E. Moerner (to be published).
[7] N. G. van Kampen, *Stochastic Processes in Physics and Chemistry* (Elsevier, New York, 1992).
[8] L. I. McCann, M. Dykman, and G. Golding, Nature (London) **402**, 785 (1999).
[9] J. E. Curtis, B. A. Koss, and D. G. Grier, Opt. Commun. **207**, 169 (2002).